Smart Structures and Systems, *Vol. 23, No. 6 (2019) 521-536*
DOI: https://doi.org/10.12989/sss.2019.23.6.521

Design formulas for vibration control of taut cables using passive MR dampers

Yuanfeng Duan[1a], Yi-Qing Ni[2b], Hongmei Zhang[*1], Billie F. Jr. Spencer[3c], Jan-Ming Ko[2d] and Yi Fang[1e]

[1]*College of Civil Engineering and Architecture, Zhejiang University, 866 Yuhangtang Rd., Hangzhou 310058, P.R. China*
[2]*Department of Civil and Environmental Engineering, The Hong Kong Polytechnic University, Hung Hom, Kowloon, Hong Kong*
[3]*Department of Civil and Environmental Engineering, The University of Illinois at Urbana-Champaign, Urbana-Champaign, Illinois, USA*

(Received August 11, 2018, Revised February 22, 2019, Accepted February 27, 2019)

Abstract. Using magnetorheological (MR) dampers in multiswitch open-loop control mode has been shown to be cost-effective for cable vibration mitigation. In this paper, a method for analyzing the damping performance of taut cables incorporating MR dampers in open-loop control mode is developed considering the effects of damping coefficient, damper stiffness, damper mass, and stiffness of the damper support. Making use of a three-element model of MR dampers and complex modal analysis, both numerical and asymptotic solutions are obtained. An analytical expression is obtained from the asymptotic solution to evaluate the equivalent damping ratio of the cable-damper system in the open-loop control mode. The individual and combined effects of the damping coefficient, damper stiffness, damper mass and stiffness of damper support on vibration control effectiveness are investigated in detail. The main thrust of the present study is to derive a general formula explicitly relating the normalized system damping ratio and the normalized damper parameters in consideration of all concerned effects, which can be easily used for the design of MR dampers to achieve optimal open-loop vibration control of taut cables.

Keywords: taut cable; vibration mitigation; MR damper; passive control; open-loop control

1. Introduction

Owing to extremely low damping, typically on the order of a fraction of one percent, cables in cable-stayed bridges are prone to vibrations with excessive amplitudes induced by support (deck and tower) motion and weather conditions (Yamaguchi and Fujino 1998). In particular, rain-wind-induced cable vibrations have been observed in a number of cable-stayed bridges around the world (Pacheco and Fujino 1993, Matsumoto *et al.* 1995, Hikami and Shiraishi 1998, Poston 1998, Verwiebe 1998, Persoon and Noorlander 1999, Tanaka 2003, Ni *et al.* 2007). The amplitude of cable vibrations during rain-wind excitation was reported to be up to 5 to 10 times the diameter of the cable. This kind of vibrations may cause reduced life of the cables and result in damage to the anchorages between the cables and deck, and therefore is a main concern in the design of cable-stayed bridges.

Transversely attached viscous/viscoelastic dampers have been implemented in numerous cable-stayed bridges to mitigate this kind of cable vibrations (Watson and Stafford 1988, Miyata 1991, Matsumoto *et al.* 1992, Takano *et al.* 1997, Virlogeux 1998, Persoon and Noorlander 1999, Main and Jones 2001, Xu *et al.* 2007, Zhou *et al.* 2014, 2018, Duan *et al.* 2018). Existing investigations (Sulekh 1990, Pacheco *et al.* 1993, Krenk 2000, Main and Jones 2002, Wang *et al.* 2005) indicate that the maximum system damping which an optimal viscous damper can achieve is limited and approximately proportional to the distance, relative to the length of the cable, between the damper and the cable anchorage. The size (or damping coefficient) of the optimal viscous damper depends on the vibration mode and on the distance between the damper and the cable anchorage relative to the cable length. Although the mechanism of rain-wind excitation is still a conundrum, it is widely accepted that the rain-wind-induced cable vibration can be mitigated if the cable damping is - sufficiently high to make the Scruton number greater than 10 (Tanaka 2003, Irwin 1997, Yamada 1997). This is the so-called Irwin's criterion. Dampers are usually attached to stay cables unobtrusively near the anchorage at the deck and thus detract minimally from the aesthetics of the bridge. For

*Corresponding author, Professor
E-mail: zhanghongmei@zju.edu.cn
[a] Professor
E-mail: ceyfduan@zju.edu.cn
[b] Chair Professor
E-mail: ceyqni@polyu.edu.hk
[c] Chair Professor
E-mail: bfs@illinois.edu
[d] Chair Professor
E-mail: cejmko@polyu.edu.hk
[e] Ph.D. Student
E-mail: 11612056@zju.edu.cn

ISSN: 1738-1584 (Print), 1738-1991 (Online)

long-span cable-stayed bridges with main span reaching 1000 m (e.g., the Stonecutters Bridge with a main span of 1018 m and the longest stays of 536 m and the Sutong Bridge with a main span of 1088 m and the longest stays of 577 m), the maximum attainable modal damping ratios when installing (optimal) viscous dampers at rational locations (e.g., 1% of the cable length) are likely to be insufficient for mitigating rain-wind-induced vibration according to the Irwin's criterion. Johnson *et al.* (1999) was the first to propose magneto-rheological (MR) dampers for semi-active cable vibration control. Subsequently, investigators have investigated MR dampers to realize more effective cable vibration mitigation (Ni *et al.* 2002, Johnson *et al.* 2003, 2007, Duan 2004, Duan, *et al.* 2005, Li *et al.* 2007, Or *et al.* 2008, Wu and Cai 2010, Kim *et al.* 2010, Zhao and Zhu 2011, Guan *et al.* 2012, Huang *et al.* 2012, 2015, Weber *et al.* 2014, Chen *et al.* 2016). Their studies show that semi-active MR dampers with the aid of an appropriate real-time closed-loop control strategy are capable of offering much better damping performance than optimal passive dampers for cable vibration control.

Apart from being effective in closed-loop control, MR dampers are found superior to viscous dampers for cable vibration mitigation even when they are used as adjustable passive dampers in open-loop control mode (Chen *et al.* 2004, Duan 2004, Duan *et al.* 2006, Weber *et al.* 2009, Zhou and Sun 2013, Wang *et al.* 2018, Zhou *et al.* 2018, Wang *et al.* 2019). Owing to different geometric configurations of cables on cable-stayed bridges, viscous dampers of the same size can only afford optimal damping to one or a few cables, while the vibration in other cables attached with the same dampers may still fail to be suppressed due to insufficient damping. However, MR dampers of the same size can provide optimal damping to each of the cables by tuning the damper voltage/current input to appropriate values. Rain-wind-induced cable vibration is typically dominated by a single low-frequency mode; however, it is currently unclear how to determine a priori the dominant mode for a given cable for which optimal damping should be sought. As a result, the design of passive (viscous) dampers is usually conducted by considering several possible modes and determining the damper size to achieve appropriate (but not necessarily optimal) damping performance for all the concerned modes, which is unalterable after the dampers are installed, even when the dominant mode is identified correctly. In contrast, although the MR dampers are designed in the same way as the passive dampers, the damping characteristic for the dominant mode can be adjusted; thus the damping performance for each individual cable can be optimized. These salient advantages have resulted in the applications of MR dampers to several cable-stayed bridges (Ko *et al.* 2003, Ou 2003, Jung *et al.* 2004, Duan *et al.* 2006). When being targeted to enhance the cable damping to suppress rain-wind-induced vibration, implementing MR dampers in open-loop control mode is more practical and economical than in closed-loop control mode.

This study attempts to present a general formula for adaptive open-loop cable vibration control using MR dampers, thus to facilitate the practical engineering applications. The essential issue is to determine the modal damping ratio of the cable-damper system taking into account the coupled effect of all involved damper and cable parameters. Previous studies provide valuable references for this study. For viscous dampers, Kovacs (1982) was first to semi-emperically identify the optimal damping coefficient of the damper. Pacheco *et al.* (1993) presented a universal estimation curve relating modal damping and damper coefficient through numerical study. Using a different approach, the complex mode analysis, Krenk (2000) obtained an analytical form of the universal design curve by Pacheco *et al.* (1993). The influence of cable sag was further studied (Krenk and Nielson, 2002). A general form was formulated by Krenk and Hogsberg (2005) to analyze the damping performances of linear viscous damper, fractional viscous damper, and nonlinear viscous damper; the influence of cable sag, support stiffness, and inertial mass of the damper was individually discussed. Main and Jones (2002a) also used the complex modes to analyze the effect of a linear viscous damper located arbitrarily along the cable, and then obtained the effect of a nonlinear viscous damper by an averaging procedure (Main and Jones 2002b). Fujino *et al.* (2008) analytically studied the effect of sag and flexural rigidity of the cable, and support stiffness of a viscous damper or high damping rubber damper, a design formula was provided. Weber *et al.* (2010) investigated Coulomb friction damper using simulation of free-decay vibration, and energy spillover to higher modes was discussed. Huang and Jones (2011) studied the effect of linear elastic spring support on cable vibration mitigation using a viscous damper or friction threshold. Considering the characteristics of stay cables and the engineering application practice, the coupled effect of cable sag, and inertial mass, support stiffness, damping coefficient, and frictional force should be investigated. The previous studies have studied effect of individual or part of the mentioned parameters. While, extension of these previous studies to the current case is not obvious or straightforward, because the effect of these parameters is coupled. Different from the work done by other investigators on cable vibration control adopting passive dampers (Main and Jones 2002, Krenk 2005), the present study is to derive a general formula taking into account the combined effect of the above-mentioned parameters and provide an approach for the design of MR dampers to achieve optimal open-loop vibration control of taut cables. Such outcomes are of significance to engineering practice.

On the basis of previous studies, this paper presents a general design formula for analyzing the damping performance of taut cables incorporating MR dampers in open-loop control mode. A three-element model (a mechanical analog of a dash-port, a spring, and a frictional element in parallel), originally proposed by Powell (1994) and validated using experimental data of a typical commercial damper (Duan 2004), is adopted to characterize the MR damper in this study. Following the method by Krenk (2004, 2005), the paper first formulate the E.O.M. of cable-MR damper system. Both analytical and numerical solutions are obtained to evaluate the equivalent modal damping ratio of the cable-damper system in open-loop

control mode considering the effects of damper stiffness, damper mass, and stiffness of damper support. With the derived analytical formula, the influence of the damper stiffness, damper mass, and stiffness of damper support on vibration control effectiveness is studied in detail.

2. Formulation

2.1 Equation of motion

As shown in Fig. 1, the cable-damper system consists of a taut cable and an MR damper connected to an elastic support with linear stiffness k_s. The length of the cable is l, the static tension force T_0, and the mass per unit length m. The MR damper is located at x_d from the left end of the cable. For convenience, a complementary length $x'_d = l - x_d$ and a complementary coordinate $x' = l - x$ are introduced as illustrated in Fig. 1.

Free oscillation of the cable assuming constant cable force is described by the partial differential equation (Krenk 2005)

$$T_0 \frac{\partial^2 y}{\partial x^2} - m\frac{\partial^2 y}{\partial t^2} = F_d \delta(x - x_d) \tag{1}$$

where $y(x,t)$ is the transverse displacement; $\delta(x-x_d)$ is the Dirac delta function, x_d specifies the location of the damper; and F_d is the damper force exerted to the cable.

The boundary conditions specifying the fixed ends can be expressed as

$$y(0,t) = 0, \quad y(l,t) = 0 \tag{2}$$

A discontinuity in the inclination of the cable is observed at the damper location, which provides a transverse force matching the damper force. The equilibrium equation at the damper location can be obtained from Eq. (1) as

$$T_0\left(\frac{\partial y}{\partial x}\Big|_{x_d^+} - \frac{\partial y}{\partial x}\Big|_{x_d^-}\right) = F_d \tag{3}$$

Although a variety of mathematical models have been proposed to characterize MR dampers (Spencer *et al.* 1997, Butz and von Stryk 2002, Jung *et al.* 2004), the three-element model proposed by Powell (1994) is adopted in the present study, because of its simplicity in expression and satisfactory accuracy in representing the characteristics of MR dampers (Duan 2004). The mechanical analogue of this model, as shown in Fig. 1, consists of three elements in parallel: a viscous dashpot with viscous coefficient c_e, a spring with stiffness coefficient k_e, and a frictional element with frictional coefficient FI in parallel. The parameters k_e, c_e, and FI depend on the vibration frequency, displacement amplitude, and voltage/current input to the MR damper. Denoting the movement of the damper piston (the upper part) and its cover (the lower part) as y_d, and y_s, the following expressions are obtained (Powell 1994)

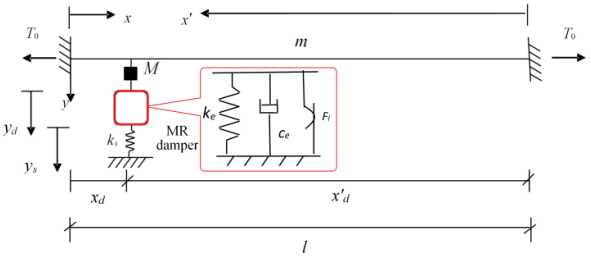

Fig. 1 Taut cable-damper system

$$F_d = M\ddot{y}_d + k_e(y_d - y_s) + c_e(\dot{y}_d - \dot{y}_s) + F_I sign(\dot{y}_d - \dot{y}_s) \tag{4a}$$

$$k_e(y_d - y_s) + c_e(\dot{y}_d - \dot{y}_s) + F_I sign(\dot{y}_d - \dot{y}_s) = k_s y_s \tag{4b}$$

where M is the concentrated mass of the piston plus the connection components between the cable and the damper. By denoting the relative movement between the damper piston and its cover as , then

$$\Delta = y_d - y_s \tag{5}$$

Assuming y_d is a specified imposed displacement, we obtain

$$\begin{aligned} y_d &= (1 + \frac{k_e}{k_s})\Delta + \frac{c_e}{k_s}\dot{\Delta} + \frac{1}{k_s}F_I \,\mathrm{sgn}(\dot{\Delta}) \\ F_d &= M\ddot{y}_d + k_e\Delta + c_e\dot{\Delta} + F_I \,\mathrm{sgn}(\dot{\Delta}) \end{aligned} \tag{6a,b}$$

When the damper is connected to the cable, $y_d(t) = y(x_d, t)$.

2.2 Complex modal analysis

Eq. (1) can be solved via complex modal analysis. By assuming harmonic response, the free vibration can be expressed as

$$\begin{aligned} y(x,t) &= \mathrm{Re}[\tilde{y}\exp(i\omega t)], \\ F_d &= \mathrm{Re}[\tilde{F}_d \exp(i\omega t)], \\ \Delta &= \mathrm{Re}[\tilde{\Delta}\exp(i\omega t)] \end{aligned} \tag{7a-c}$$

where $\tilde{y}(x)$ is the complex mode shape; ω is the corresponding complex circular frequency; $\tilde{\Delta}$ is the complex modulus of the relative displacement Δ between the damper piston (the upper part) and the cover (the lower part); $\tilde{F}_d$ is the complex modulus of damper force F_d. By combining Eqs. (7(a)) and (1), the complex mode shape should satisfy the differential equation

$$\frac{d^2\tilde{y}}{dx^2} + \beta^2\tilde{y} = 0, \quad \begin{cases} 0 < x < x_d \\ 0 < x' < x'_d \end{cases} \tag{8}$$

where β is the complex wavenumber defined as

$$\beta = \omega\sqrt{m/T_0} \tag{9}$$

With regard to the homogeneous Eq. (8), for each of the two intervals between the damper and the cable ends, the complex mode shape can be easily solved as

$$\tilde{y} = \begin{cases} \tilde{y}_d \dfrac{\sin(\beta x)}{\sin(\beta x_d)}, & 0 \le x \le x_d \\ \tilde{y}_d \dfrac{\sin(\beta x')}{\sin(\beta x'_d)}, & 0 \le x' \le x'_d \end{cases} \tag{10}$$

by considering the boundary conditions given in Eq. (2) and the continuity of the shape function at the damper location $x = x_d$, where $\tilde{y}_d$ is the displacement amplitude at the damper location to be determined. For brevity and without loss of generality, the amplitude $\tilde{y}_d$ is chosen to be purely real. Using the equivalent energy method (Weber and Boston 2010, Huang and Jones 2011), an equivalent damping coefficient for frictional force can be obtained

$$\begin{aligned} &\mathrm{W} = \int_0^T F_I \,\mathrm{sgn}(\dot{\Delta})\cdot\dot{\Delta}\,dt = 4F_I\|\Delta\| \\ &\mathrm{W} = \int_0^T c_I\,\dot{\Delta}\cdot\dot{\Delta}\,dt = c_I\pi\|\dot{\Delta}\|\|\Delta\| \\ &c_I = \frac{4F_I}{\pi\|\dot{\Delta}\|} \end{aligned} \tag{11a-c}$$

where, c_I is the equivalent viscous coefficient of frictional force; $\|\dot{\Delta}\|$ is the velocity amplitude of damper motion; $\|\Delta\|$ is the displacement amplitude of damper motion, W is the energy dissipated within one cycle by dampers.

Substituting Eq. (7(b)) and (7(c)) into Eq. (6) and replacing $F_I\,sgn(\dot{\Delta})$ by $c_I\dot{\Delta}$ leads to

$$\begin{aligned} &\tilde{y}_d = \left\{1+\frac{1}{k_s}\left[k_e + c_e\cdot(i\omega) + c_I\cdot(i\omega)\right]\right\}\tilde{\Delta} \\ &\tilde{F}_d = -M\omega^2\tilde{y}_d + \left[k_e + c_e(i\omega) + c_I\cdot(i\omega)\right]\tilde{\Delta} \end{aligned} \tag{12a,b}$$

Substituting Eqs. (7), (10) into Eq. (3) yields the equation for the complex eigenfrequency, which is expressed as

$$\cot(\beta x_d) + \cot(\beta x_d') = -\frac{1}{T_0\beta}\frac{\tilde{F}_d}{\tilde{y}_d} \tag{13}$$

Eq. (13) can be re-arranged as

$$\tan(\beta l) = \frac{\sin^2(\beta x_d)\dfrac{1}{T_0\beta}\dfrac{\tilde{F}_d}{\tilde{y}_d}}{1+\cos(\beta x_d)\sin(\beta x_d)\dfrac{1}{T_0\beta}\dfrac{\tilde{F}_d}{\tilde{y}_d}} \tag{14}$$

Eqs. (13) and (14) provide solution for the wavenumber, from which the modal frequency and damping ratio can be obtained. In particular, Eq. (14) is suitable for solution either in asymptotic form or by numerical iteration, as discussed later. As a matter of fact, by substituting the relationship between $\tilde{F}_d$ and $\tilde{y}_d$ for a specific damper into Eq. (14), the wavenumber for any taut cable-damper system can be calculated. Hence, this equation provides a basis for evaluating the effectiveness of a damper and for designing a damper to achieve the desired control performance. Combining Eqs. (14) and (12), we obtain the solution for the wavenumber for the cable-damper system as

$$\tan(\beta l) = \frac{\dfrac{1}{T_0\beta}\sin^2(\beta x_d)\left[A-(1+\dfrac{1}{k_s}A)M\omega^2\right]}{(1+\dfrac{1}{k_s}A)+\dfrac{1}{T_0\beta}\cos(\beta x_d)\sin(\beta x_d)\left[A-(1+\dfrac{1}{k_s}A)M\omega^2\right]} \tag{15}$$

where

$$A = k_e + ic_e\omega + ic_I\omega \tag{16}$$

The wavenumber is denoted as β_n (n = 1, 2, 3…) and the corresponding eigenfrequencies as ω_n, whose relationship is defined in Eq. (9). The eigenfrequencies can be represented as

$$\omega_n = \|\omega_n\|(\sqrt{1-\xi_n^2} + i\xi_n) \tag{17}$$

of which the real part represents the frequency attenuation due to damping and the imaginary part implies the modal damping ratio ξ_n, while the modulus describes the magnitude of the angular frequency. The modal damping ratio can be obtained by

$$\xi_n = \left(1+\frac{\mathrm{Re}(\omega_n)^2}{\mathrm{Im}(\omega_n)^2}\right)^{-\frac{1}{2}} \approx \frac{\mathrm{Im}(\omega_n)}{\mathrm{Re}(\omega_n)} = \frac{\mathrm{Im}(\beta_n)}{\mathrm{Re}(\beta_n)} \tag{18}$$

The relative error of the approximation in Eq. (18) is less than 0.5% for $\xi_n \le 10\%$ and less than 0.13% for $\xi_n \le 5\%$, so it is accurate enough for actual cable-damper systems whose damping ratios are usually less than 5% of critical. In the following, we explore numerical and asymptotic solutions for the wavenumber and eigenfrequency of the cable-damper system.

2.3 Numerical solution

Eq. (15) can be iteratively solved by substituting the current estimate β_n^j (j = 0, 1, 2, …) into the right-hand side of Eq. (15) and obtaining a new estimate β_n^{j+1} from the left-hand side of Eq. (15). The iterative scheme is expressed as

$$\beta_n^{j+1}l = n\pi + \arctan\left\{\frac{\dfrac{1}{T_0\beta_n^j}\sin^2(\beta_n^j x_d)\left[A^j-(1+\dfrac{A^j}{k_s})M(\omega_n^j)^2\right]}{(1+\dfrac{A^j}{k_s})+\dfrac{1}{T_0\beta_n^j}\cos(\beta_n^j x_d)\sin(\beta_n^j x_d)\left[A^j-(1+\dfrac{A^j}{k_s})M(\omega_n^j)^2\right]}\right\} \tag{19}$$

where j is the iteration number, and

$$A^j = k_e + ic_e\omega_n^j + ic_I\omega_n^j \tag{20}$$

For brevity, dimensionless parameters η_c, η_I, u_k, u_s, γ_M are introduced to normalize the damper viscous coefficient c_e, damper frictional coefficient F_I, damper stiffness k_e, stiffness of damper support k_s, and damper mass M as

$$\begin{aligned} &\eta_c = \frac{c_e}{\sqrt{T_0 m}},\ \eta_I = \frac{c_I}{\sqrt{T_0 m}},\ u_k = \frac{n\pi k_e}{\omega_n^0\sqrt{T_0 m}} = \frac{k_e}{T_0} \\ &u_s = \frac{n\pi k_s}{\omega_n^0\sqrt{T_0 m}} = \frac{k_s l}{T_0},\ \gamma_M = \frac{n^2\pi^2 M}{ml} = \frac{M(\omega_n^0)^2 l}{T_0} \end{aligned} \tag{21a-e}$$

Deploying the above dimensionless parameters, Eq. (19) becomes

$$\beta_n^{j+1}l = n\pi + \arctan\frac{\sin^2\left[(\beta_n^j l)\dfrac{x_d}{l}\right]\left[D^j - E^j F^j\right]}{E^j + \cos\left[(\beta_n^j l)\dfrac{x_d}{l}\right]\sin\left[(\beta_n^j l)\dfrac{x_d}{l}\right]\left[D^j - E^j F^j\right]} \tag{22}$$

where

$$D^j = \frac{A^j}{T_0\beta_n^j} = \frac{u_k}{(\beta_n^j l)} + i(\eta_c + \eta_l)$$

$$E^j = 1 + \frac{A^j}{k_s} = 1 + \frac{1}{u_s}\left[u_k + i(\eta_c + \eta_l)\beta_n^j l\right] \quad (23a\text{-}c)$$

$$F^j = \frac{M(\omega_n^j)^2}{T_0\beta_n^j} = \frac{\beta_n^j l}{(\beta_n^0 l)^2}\gamma_M = \frac{\beta_n^j l}{n^2\pi^2}\gamma_M$$

The initial guesses for iterative solution of the wavenumber and circular frequency can be taken as those of the undamped taut cable, which are expressed as

$$\beta_n^0 = \frac{n\pi}{l}, n = 1, 2, 3, \ldots \quad (24)$$

and

$$\omega_n^0 = \frac{n\pi}{l}\sqrt{\frac{T_0}{m}}, n = 1, 2, 3, \ldots \quad (25)$$

Once the values of β_n or ω_n are obtained, the damping ratio of the cable-damper system can be determined by Eq. (18).

2.4 Numerical solution

Perturbation methods are applied to obtain an asymptotic solution. For the undamped taut cable, the wavenumbers and circular frequencies have been obtained in Eqs. (24) and (25). Supposing the wavenumber solution β_n of the damped taut cable be a small perturbation from β_n^0, we have

$$\tan(\beta_n l) = \tan(\beta_n l - n\pi) \approx \beta_n l - n\pi = \beta_n l - \beta_n^0 l = \Delta\beta_n l \quad (26)$$

Substituting Eqs. (24) to (26) into Eq. (15) leads to the following asymptotic formula

$$\beta l \approx n\pi\left[1 + \frac{S^2\left[B + in\pi(\eta_c + \eta_l)\left(1 - \frac{\gamma_M}{u_s}\right)\right]\frac{x_d}{l}}{\left(1 + \frac{u_k}{u_s} + BCS\frac{x_d}{l}\right) + in\pi(\eta_c + \eta_l)\left[\frac{1}{u_s} + \left(1 - \frac{\gamma_M}{u_s}\right)CS\frac{x_d}{l}\right]}\frac{x_d}{l}\right] \quad (27)$$

where

$$B = u_k\left(1 - \frac{\gamma_M}{u_s}\right) - \gamma_M, \quad C = \cos(n\pi\frac{x_d}{l}), \quad S = \frac{\sin(n\pi\frac{x_d}{l})}{n\pi\frac{x_d}{l}} \quad (28a\text{-}c)$$

When the damper location is close to one cable end, i.e., $\frac{x_d}{l} << 1$, combining Eqs. (18) and (27) yields

$$\frac{\frac{\xi_n}{x_d}}{l} = \frac{n\pi(\eta_c + \eta_l)S^2\frac{x_d}{l}}{\left[1 + \frac{u_k}{u_s} + BCS\frac{x_d}{l}\right]^2 + \left[n\pi(\eta_c + \eta_l)\left(\frac{1}{u_s} + (1 - \frac{\gamma_M}{u_s})CS\frac{x_d}{l}\right)\right]^2} \quad (29)$$

where *B*, *C* and *S* are defined in Eq. (28). In the case of $\frac{m_d}{l} << 1$, there exist the following approximations

$$\sin(\beta_n^0 x_d) = \sin(n\pi\frac{x_d}{l}) \approx n\pi\frac{x_d}{l} \quad (30a,b)$$

$$\cos(\beta_n^0 x_d) = \cos(n\pi\frac{x_d}{l}) \approx 1$$

i.e.,

$$S \approx 1, C \approx 1 \quad (31a,b)$$

By using different approximations, we can obtain four asymptotic solutions

$$\xi_n^I = \xi_n(S, C), \quad \xi_n^{II} = \xi_n(1, C) \quad (32a,b)$$

$$\xi_n^{III} = \xi_n(S, 1), \quad \xi_n^{IV} = \xi_n(1, 1) \quad (32c,d)$$

ξ_n^I keeps the form of Eq. (29); ξ_n^{II} is obtained by replacing *S* as 1 in Eq. (29); ξ_n^{III} is obtained by replacing *C* as 1 in Eq. (29); and ξ_n^{IV} is obtained by replacing both *S* and *C* as 1 in Eq. (29). The accuracy of the four asymptotic solutions will be studied in the next section.

3. Validation of the solution

The numerical solution will first be validated by comparing it with the results obtained by other researchers with respect to a special case of an ideal viscous damper with ideal support. Then the accuracy of the asymptotic solution is verified by comparing it with the numerical solution.

3.1 Numerical solution

Pacheco *et al.* (1993) proposed a 'universal curve' for design of viscous dampers for passive cable vibration control by neglecting the damper mass, damper stiffness, and support stiffness $(\frac{1}{u_s} = \eta_l = \gamma_M = u_k = 0)$. The 'universal curve' can be used graphically in choosing proper size and location of the damper for required amount of additional damping in a specific mode, and estimating the additional damping at different modes for a given damper coefficient and location. However, to accurately calculate this 'universal curve', it is necessary to include several hundred terms of sinusoidal shape functions, identical to the mode shapes of the free cable. To expedite the calculation convergence, Johnson *et al.* (1999) proposed to use one static deflection function plus sine series as the shape functions. They showed that, when the static deflection function was used as the first shape function, only a few sine terms were required for the convergence of damping calculation. We first compare the present numerical solution with the results obtained by Pacheco *et al.* (1993) and Johnson *et al.* (1999) for the ideal viscous damper case.

By judiciously grouping various parameters (modal damping ratio, mode number, damper coefficient, damper location, cable length, mass per unit length and fundamental frequency of the cable), the normalized damping ratio of the cable and the normalized damper coefficient are defined as (Pacheco *et al.* 1993)

$$\bar{\xi} = \frac{\xi}{x_d/l} \quad (33)$$

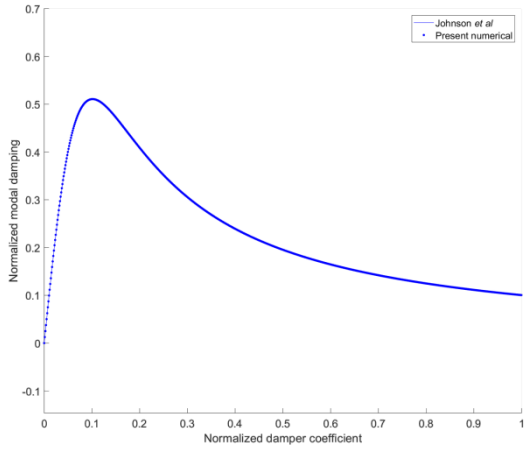

Fig. 2 Comparison of numerical solution with 'universal curve' (x_d/l = 0.05, 1st mode)

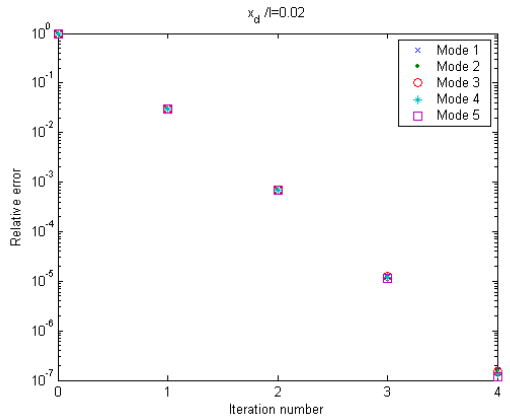

Fig. 3 Evolution of relative error with iteration number ($x_d/l = 0.02$, $\kappa = 0.1$)

$$\kappa = \frac{c_e}{ml\omega_1^0}\cdot n\cdot\frac{x_d}{l} = \frac{c_e}{\pi\sqrt{Tm}}\cdot n\cdot\frac{x_d}{l} = \frac{1}{\pi}\eta_c n\frac{x_d}{l} \tag{34}$$

Fig. 2 illustrates the 'universal curve' of the normalized damping ratio versus the normalized damper coefficient for the first mode when $\frac{x_d}{l}=0.05$, obtained by the present numerical solution procedure, the Pacheco's method (Pacheco *et al.* 1993), and the Johnson's method (Johnson *et al.* 1999) when using a static deflection shape plus 50 sine terms. Good agreement is observed between the results obtained by different methods. The curves for the normalized damping ratio versus the normalized damper coefficient for higher modes are also obtained and a similar observation is made (Duan 2004). To understand the iterative convergence of the proposed numerical solution procedure, Fig. 3 plots the evolution of the relative error with iteration number for the first five modes when x_d/l=0.02 and κ=0.1. The relative error is defined as

$$e_\xi = \frac{\left|\xi^i - \xi^{1000}\right|}{\xi^{1000}} \tag{35}$$

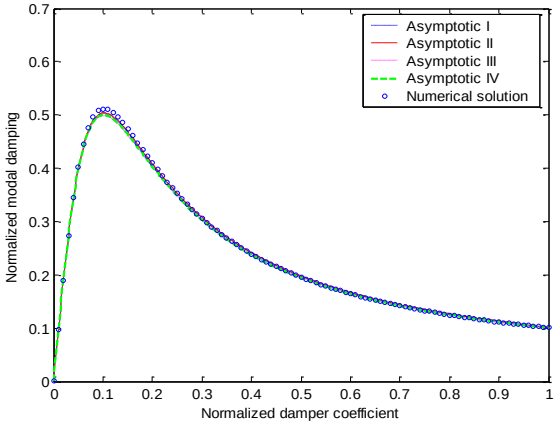

Fig. 4 Comparison of asymptotic solutions with numerical solution (x_d/l = 0.02, 2nd mode)

ξ^{1000} is the damping ratio obtained after 1000 iterations. It is seen from Fig. 3 that the relative error approaches to around 10^{-3} after the second iteration. Therefore, the proposed numerical procedure is computationally efficient in obtaining accurate solutions.

3.2 Asymptotic solution

Fig. 4 shows the normalized damping ratio versus the normalized damper coefficient for the second mode when $\frac{x_d}{l}=0.02$, obtained by the asymptotic and numerical solution procedures.

The relative errors for all the four asymptotic solutions are found less than 2.3%. In this case the simplest asymptotic solution ξ^{IV} can be used for damper design, i.e.,

$$\frac{\frac{\xi_n}{x_d}}{l} = \frac{n\pi(\eta_c+\eta_I)\frac{x_d}{l}}{\left[1+\frac{u_k}{u_s}+B\frac{x_d}{l}\right]^2+\left[n\pi(\eta_c+\eta_I)\left(\frac{1}{u_s}+(1-\frac{\gamma_M}{u_s})\frac{x_d}{l}\right)\right]^2} \tag{36}$$

where B is defined in Eq. (28). It should be noted that Eq. (36) is applicable only to the case of $\frac{nx_d}{l}<<1$. When $\frac{nx_d}{l}$ is large, the expression of $\xi(S,C)$ must be utilized for accurate evaluation; Duan has determined the values of S and C for different ranges of $\frac{nx_d}{l}$ by means of a nonlinear curve-fitting technique (Duan 2004).

4. Analysis of damping performance

With the asymptotic solution, we can explicitly analyze the effects of damper viscous and frictional coefficients, damper stiffness, damper mass and stiffness of damper support on the cable vibration control effectiveness. First, Eq. (29) is rewritten as

$$\frac{\xi_n}{\frac{x_d}{l}}=\frac{n\pi(\eta_c+\eta_I)S^2\frac{x_d}{l}}{\left[1+(u_kG-\gamma_MCS)\frac{x_d}{l}\right]^2+\left[n\pi(\eta_c+\eta_I)G\frac{x_d}{l}\right]^2} \tag{37}$$

where

$$G=\left(\frac{1}{u_s}+(1-\frac{\gamma_M}{u_s})CS\frac{x_d}{l}\right)\Big/\frac{x_d}{l}=\left(\frac{1}{u_s}(1-\gamma_MCS\frac{x_d}{l})+CS\frac{x_d}{l}\right)\Big/\frac{x_d}{l} \tag{38}$$

From Eq. (37), it is seen that the system modal damping ratio is decreased with the increase of the damper stiffness u_k, as G is independent of u_k. It is known from Eq. (38) that when $u_s\to\infty$, $G\to CS$.

Similarly, Eq. (29) can be rewritten as

$$\frac{\xi_n}{\frac{x_d}{l}}=\frac{n\pi(\eta_c+\eta_I)S^2\frac{x_d}{l}}{\left[1+\left(u_kH-(1+\frac{u_k}{u_s})\gamma_MCS\right)\frac{x_d}{l}\right]^2+\left[n\pi(\eta_c+\eta_I)\left(H-\frac{1}{u_s}CS\gamma_M\right)\frac{x_d}{l}\right]^2} \tag{39}$$

where

$$H=\left(\frac{1}{u_s}+CS\frac{x_d}{l}\right)\Big/\frac{x_d}{l} \tag{40}$$

It is seen from Eq. (39) that the damper mass γ_M counteracts the effect of the damper stiffness u_k, and therefore is beneficial for system damping enhancement.

When

$$\left(u_kH-(1+\frac{u_k}{u_s})\gamma_MCS\right)=0 \tag{41}$$

the negative effect of the damper stiffness u_k will be neutralized by the positive effect of the damper mass γ_M within the applicable range of Eq. (29) in case of $u_s\to\infty$. If the cable vibration frequency is obviously altered by the concentrated damper mass, the damping enhancement should be numerically computed using Eq. (19) or (22).

To investigate the effect of support stiffness u_s, Eq. (29) is rewritten again as

$$\frac{\xi_n}{\frac{x_d}{l}}=\frac{n\pi(\eta_c+\eta_I)S^2\frac{x_d}{l}}{\left[1+\left((\frac{1}{u_s}N+CS)u_k-\gamma_MCS\right)\frac{x_d}{l}\right]^2+\left[n\pi(\eta_c+\eta_I)\left(\frac{1}{u_s}N+CS\right)\frac{x_d}{l}\right]^2} \tag{42}$$

where

$$N=\left(1-\gamma_MCS\frac{x_d}{l}\right)\Big/\frac{x_d}{l} \tag{43}$$

It is clear that the maximum attainable damping ratio will decrease as $\frac{1}{u_s}$ increases. When $\frac{1}{u_s}\to 0$, it becomes the case of ideal support; when $\frac{1}{u_s}\to\infty$, corresponding to the removal of the damper, there will be no damping added to the cable.

For the damper viscous and frictional coefficients c_e and F_I, or the dimensionless parameters η_c and η_I, there is an optimal value to achieve the maximum attainable damping ratio. By letting

$$\frac{\partial\xi_n^I}{\partial(\eta_c+\eta_I)}=0 \tag{44}$$

we obtain the optimal damper coefficient

$$(\eta_c+\eta_I)_{opt}=\frac{1+(u_kG-\gamma_MCS)\frac{x_d}{l}}{n\pi G\frac{x_d}{l}}=\frac{1}{n\pi\left(\frac{1}{u_s}+\frac{CS\frac{x_d}{l}}{1-\gamma_MCS\frac{x_d}{l}}\right)}+\frac{u_k}{n\pi} \tag{45}$$

and the maximum attainable damping ratio

$$\frac{\xi_{n,opt}}{\frac{x_d}{l}}=\frac{S^2}{2G\left[1+(u_kG-\gamma_MCS)\frac{x_d}{l}\right]} \tag{46}$$

or

$$\frac{\xi_{n,opt}}{\frac{x_d}{l}}=\frac{S^2}{2\left[1+\left(u_kH-(1+\frac{u_k}{u_s})\gamma_MCS\right)\frac{x_d}{l}\right]\left[\left(H-\frac{1}{u_s}\gamma_MCS\right)\right]} \tag{47}$$

or

$$\frac{\xi_n}{\frac{x_d}{l}}=\frac{S^2}{2\left[1+\left((\frac{1}{u_s}N+CS)u_k-\gamma_MCS\right)\frac{x_d}{l}\right]\left[\left(\frac{1}{u_s}N+CS\right)\right]} \tag{48}$$

where G, defined in Eq. (38), is independent of u_k; H, defined in Eq. (40), is independent of γ_M; and N, defined in Eq. (43), is independent of us. It is clear from Eq. (45) that the value of the optimal damper coefficient increases with increasing damper stiffness u_k, decreases with increasing damper mass γ_M, and also decreases with softening of the damper support (increasing $\frac{1}{u_s}$). It is seen from Eqs. (46) to (48) that the damper stiffness u_k decreases the maximum attainable damping ratio; the damper mass γ_M counteracts the effect of the damper stiffness; and softening of the damper support (increase of $\frac{1}{u_s}$) also decreases the maximum attainable damping ratio.

A more detailed analysis on individual and combined effects of the damper stiffness, damper mass, and stiffness of damper support is given below.

4.1 Damper stiffness

For brevity and without loss of generality, we consider the effect of the damper stiffness in the case that there is no concentrated mass but ideal support, i.e., $u_s=\infty$ and $\gamma_M=0$. In this case, Eq. (37) becomes

$$\frac{\xi_n}{\frac{x_d}{l}}=\frac{n\pi(\eta_c+\eta_I)S^2\frac{x_d}{l}}{\left[1+u_kCS\frac{x_d}{l}\right]^2+\left[n\pi(\eta_c+\eta_I)CS\frac{x_d}{l}\right]^2} \tag{49}$$

The modal damping ratio in the case of no damper stiffness is obtained as

$$\frac{\xi_n}{\frac{x_d}{l}}|(u_k=0)=\frac{n\pi(\eta_c+\eta_I)S^2\frac{x_d}{l}}{1+\left[n\pi(\eta_c+\eta_I)CS\frac{x_d}{l}\right]^2} \tag{50}$$

By defining an equivalent reduced damper distance

$$\frac{x_d^{*-}}{l}=\frac{1}{1+u_kCS\frac{x_d}{l}}\frac{x_d}{l}=\frac{1}{1+CS\frac{k_ex_d}{T}}\frac{x_d}{l} \tag{51}$$

Eq. (49) can be re-expressed as

$$\frac{\frac{\xi_n}{x_d^{*-}}}{l}=\frac{n\pi(\eta_c+\eta_I)S^2\frac{x_d^{*-}}{l}}{1+\left[n\pi(\eta_c+\eta_I)CS\frac{x_d^{*-}}{l}\right]^2} \tag{52}$$

By comparing Eqs. (52) and (50), it is revealed that the effect of the damper stiffness on the system damping performance is equivalent to replacing the damper distance x_d by a reduced distance x_d^{*-}, thus decreasing the attainable damping ratio of the cable- damper system.

Next the maximum attainable damping ratio and the optimal damper coefficient are explored. When $u_s=\infty$ and $\gamma_M=0$, Eqs. (45) and (46) reduce to

$$(\eta_c+\eta_I)_{opt}=\frac{1}{n\pi CS\frac{x_d}{l}}+\frac{u_k}{n\pi}=\frac{1}{n\pi CS\frac{x_d^{*-}}{l}} \tag{53}$$

$$\frac{\xi_{n,opt}}{\frac{x_d}{l}}=\frac{S}{2C}\frac{1}{\left[1+u_kCS\frac{x_d}{l}\right]} \quad \text{or} \quad \frac{\frac{\xi_{n,opt}}{x_d^{*-}}}{l}=\frac{S}{2C} \tag{54}$$

From Eq. (53), we obtain

$$\begin{aligned}(\eta_c+\eta_I)_{opt}&=(\eta_c+\eta_I)_{opt|u_k=0}(1+u_kCS\frac{x_d}{l})\\&=(\eta_c+\eta_I)_{opt|u_k=0}(1+CS\frac{k_ex_d}{T})\end{aligned} \tag{55}$$

By generalizing Eq. (34) to

$$\kappa=\frac{1}{\pi}(\eta_c+\eta_I)n\frac{x_d}{l} \tag{56}$$

We obtain, from Eq. (55), the optimal damper coefficient as

$$\kappa_{opt}=\kappa_{opt|u_k=0}(1+u_kCS\frac{x_d}{l})=\kappa_{opt|u_k=0}(1+CS\frac{k_ex_d}{T}) \tag{57}$$

where

$$\kappa_{opt|u_k=0}=\frac{1}{\pi^2CS} \tag{58}$$

It is seen from Eqs. (55) and (57) that the optimal damper coefficient is increased by a factor $\left(1+u_kCS\frac{x_d}{l}\right)$ or $\left(1+CS\frac{k_ex_d}{T}\right)$.

From Eq. (54), we obtain

$$\xi_{n,opt}=\xi_{n,opt|u_k=0}\frac{1}{\left(1+u_kCS\frac{x_d}{l}\right)} \tag{59}$$

It is clear from Eq. (59) that, similar to the reduced damper distance x_d^{*-}, the maximum attainable damping ratio is reduced by a factor $\frac{1}{\left(1+u_kCS\frac{x_d}{l}\right)}$.

Fig. 5 shows the effect of damper stiffness on the normalized damping ratio $\xi/(x_d/l)$ versus the normalized damper coefficient κ for the second mode when $x_d/l=0.02$, $\frac{1}{u_s}$ and $\gamma_M=0$. Plotted in Fig. 5(a) are the results obtained by the numerical procedure for the damper stiffness u_k = 0, 10, 20, …, 100, respectively, with an arrow indicating the trend of increasing damper stiffness. The line with dots links the peak points of the curves, indicating the change in the maximum damping ratio and the optimal damper coefficient. It evidences that the damper stiffness reduces the maximum attainable damping ratio and increases the optimal damper coefficient. Fig. 5(b) gives a comparison of the asymptotic and numerical solutions for u_k = 0, 30, 60, and 100. The asymptotic solution shows a negligible difference from the numerical solution.

Fig. 6 shows the effect of damper stiffness on the maximum damping ratio and the optimal damper coefficient. It is observed that the maximum damping ratio decreases quadratically with increasing u_kx_d/l, while the normalized optimal damper coefficient increases linearly with the increase of u_kx_d/l. The larger u_kx_d/l is, the smaller the maximum damping ratio, and the larger the optimal damper coefficient. When u_kx_d/l is equal to 0.2, i.e., u_k = 10 for x_d/l = 0.02, the maximum attainable damping ratio is reduced by 20% of the original, from 0.51 to 0.43; and the normalized optimal damper coefficient is increased by 20%, from 0.10 to 0.12. When u_kx_d/l is equal to 0.6, the maximum attainable damping ratio is reduced by 40%, and the normalized optimal damper coefficient is increased by 60%. In this case, ignoring the effect of damper stiffness will lead to a significant discrepancy. Recalling the definition of u_k in Eq. (21), it is known that the effect of damper stiffness will be enhanced for flexible cables with long length and small tension. As the abscissa in Fig. 6 is u_kx_d/l, the effect of damper stiffness tends to be more significant when x_d/l is larger. The asymptotic results agree well with the numerical ones, validating the applicability of Eqs. (55) and (56) for evaluating the optimal damper coefficients and Eq. (59) for evaluating the maximum attainable damping ratio.

4.2 Damper mass

When the damper is ideally supported ($\frac{1}{u_s}=0$), Eq. (39) becomes

$$\frac{\xi_n}{\frac{x_d}{l}}=\frac{n\pi(\eta_c+\eta_I)S^2\frac{x_d}{l}}{\left[1+(u_k-\gamma_M)CS\frac{x_d}{l}\right]^2+\left[n\pi(\eta_c+\eta_I)CS\frac{x_d}{l}\right]^2} \tag{60}$$

If $u_k = 0$, the above equation reduces to

$$\frac{\xi_n}{\frac{x_d}{l}}|(u_k=0)=\frac{n\pi(\eta_c+\eta_I)S^2\frac{x_d}{l}}{\left[1-\gamma_M CS\frac{x_d}{l}\right]^2+\left[n\pi(\eta_c+\eta_I)CS\frac{x_d}{l}\right]^2} \tag{61}$$

By comparing Eqs. (61) and (49), $(-\gamma_M)$ plays the same role with u_k, or that the damper mass γ_M acts opposite to the damper stiffness u_k. It is seen from Eq. (60) that when $u_k=\gamma_M$ the unfavorable effect of the damper stiffness u_k can be neutralized by the damper mass γ_M. Similar to the equivalent reduced damper distance x_d^{*-}, an equivalent enlarged damper distance x_d^{*+} can be defined as

$$\frac{x_d^{*+}}{l}=\frac{1}{1-\gamma_M CS\frac{x_d}{l}}\frac{x_d}{l}=\frac{1}{1-\frac{n^2\pi^2 M}{ml}CS\frac{x_d}{l}}\frac{x_d}{l}=\frac{1}{1-CS\frac{M(\omega_n^0)^2x_d}{T_0}}\frac{x_d}{l} \tag{62}$$

which satisfies

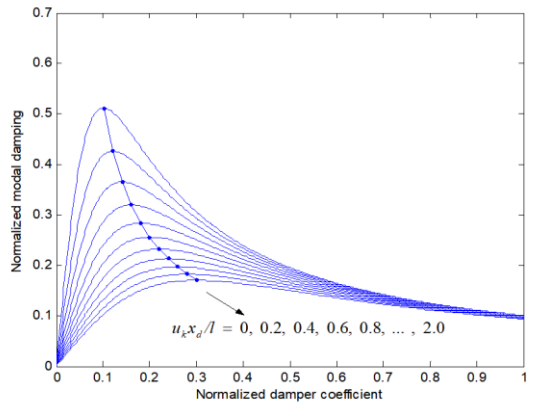

(a) Numerical solution

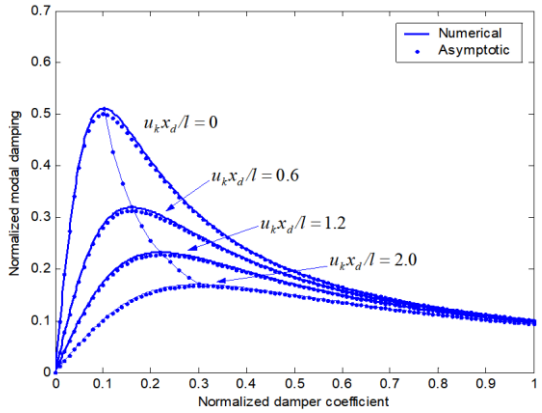

(b) Comparison of numerical and asymptotic solutions

Fig. 5 Effect of damper stiffness on 'universal curve' (x_d/l = 0.02, 2nd mode)

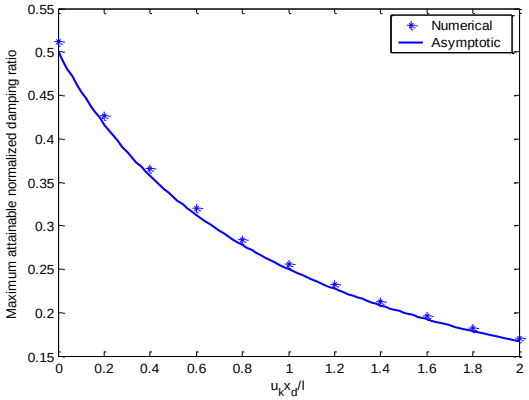

(a) Maximum attainable damping ratio

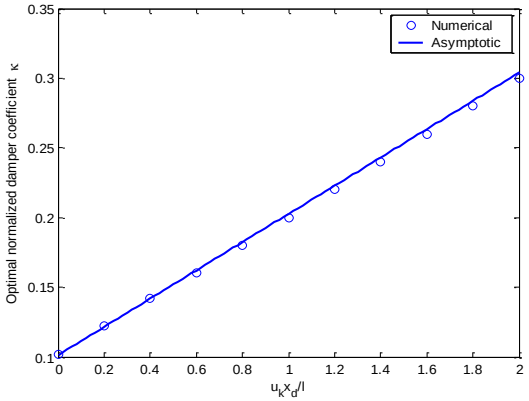

(b) Optimal damper coefficient

Fig. 6 Effect of damper stiffness on damping performance (x_d/l = 0.02, 2nd mode)

$$\frac{\xi_n}{\frac{x_d^{*+}}{l}}=\frac{n\pi(\eta_c+\eta_I)S^2\frac{x_d^{*+}}{l}}{1+\left[n\pi(\eta_c+\eta_I)CS\frac{x_d^{*+}}{l}\right]^2} \tag{63}$$

From Eq. (62), it is evident that the damper mass will play a more significant role for higher modes than lower modes. By comparing Eqs. (63) and (61), it is known that the effect of the damper mass is equivalent to an increase in the damper distance from x_d to x_d^{*+}.

The optimal damper coefficient and the maximum attainable damping ratio in the case of $\frac{1}{u_s}$ and $u_k = 0$ can be obtained from Eqs. (45) and (47) as

$$\begin{aligned}(\eta_c+\eta_I)_{opt}&=\frac{1}{n\pi CS\frac{x_d}{l}}\left(1-\gamma_M CS\frac{x_d}{l}\right)\\&=(\eta_c+\eta_I)_{opt|_{\gamma_M=0}}(1-\gamma_M CS\frac{x_d}{l})\end{aligned} \tag{64}$$

$$\frac{\xi_{n,opt}}{\frac{x_d}{l}}=\frac{S^2}{2\left(1-\gamma_M CS\frac{x_d}{l}\right)}\quad\text{or}\quad\frac{\xi_{n,opt}}{\frac{x_d^{*+}}{l}}=\frac{S}{2C} \tag{65}$$

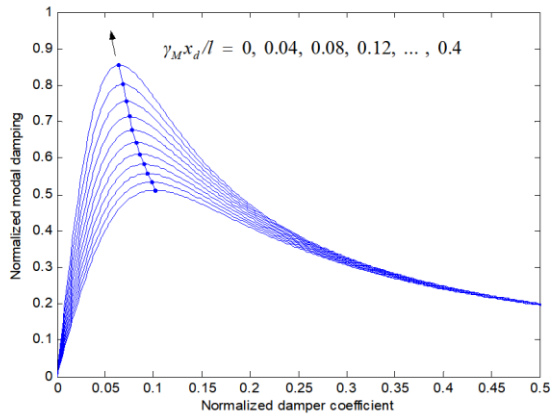

(a) Numerical solution

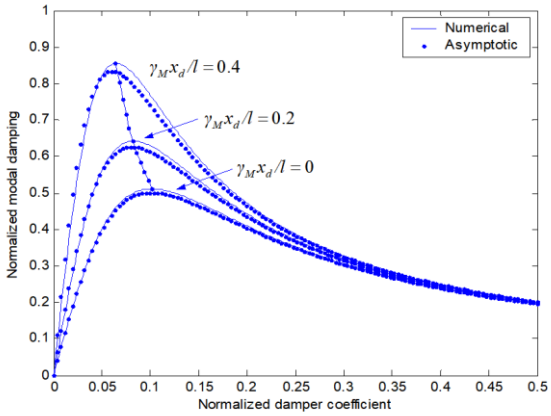

(b) Comparison of numerical and asymptotic solutions

Fig. 7 Effect of damper mass on 'universal curve' (x_d/l = 0.02, 2nd mode)

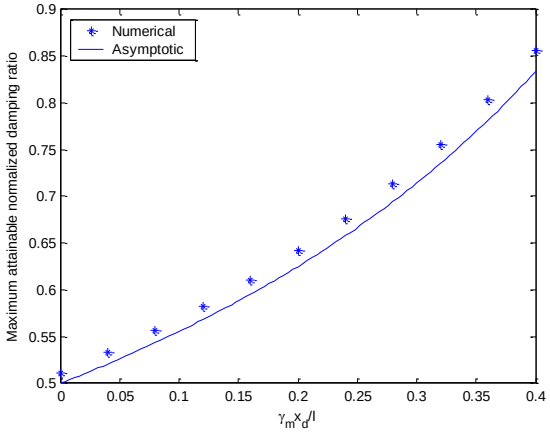

(a) Maximum attainable damping ratio

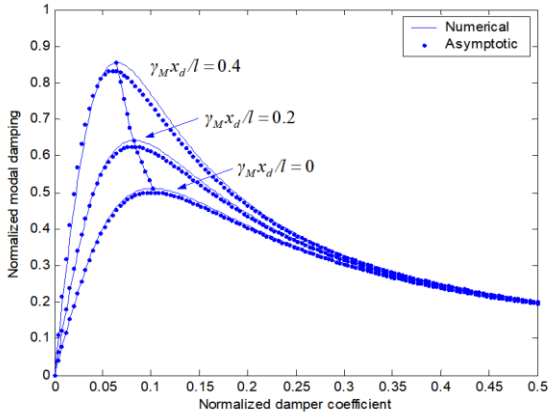

(b) Optimal damper coefficient

Fig. 8 Effect of damper mass on damping performance (x_d/l = 0.02, 2nd mode)

By combining Eqs. (64) and (56), we obtain the normalized optimal damper coefficient as

$$\kappa_{opt} = \frac{1}{\pi^2 CS}\left(1-\gamma_M CS\frac{x_d}{l}\right) \tag{66}$$

From Eqs. (64) and (66), it is evident that the optimal damper coefficient is decreased due to the damper mass by a factor $\left(1-\gamma_M CS\frac{x_d}{l}\right)$, while the maximum damping ratio is increased due to the damper mass by a factor $\left(1-\gamma_M CS\frac{x_d}{l}\right)$.

Fig. 7 shows the effect of damper mass on the normalized damping ratio $\xi/(x_d/l)$ versus the normalized damper coefficient κ for the second mode when $\frac{x_d}{l}=0.02$, $\frac{1}{u_s}=0$ and u_k = 0. Plotted in Fig. 7(a) are the results obtained by the numerical procedure for the damper mass γ_M = 0, 2, 4,…, 20, respectively, with an arrow indicating the trend of increasing damper mass. The line with dots links the peak points of the curves, indicating the change in the maximum damping ratio and the optimal damper coefficient. It evidences that the damper mass increases the maximum attainable damping ratio and decreases the optimal damper coefficient. Fig. 7(b) shows a comparison of the asymptotic and numerical solutions for γ_M = 0, 10, and 20. The asymptotic solution agrees favorably with the numerical solution.

Fig. 8 shows the effect of damper mass on the maximum damping ratio and the optimal damper coefficient. It is observed that the maximum damping ratio increases parabolically with increasing $\gamma_M x_d/l$, while the normalized optimal damper coefficient decreases nearly linearly with the increase of $\gamma_M x_d/l$. The larger $\gamma_M x_d/l$ is, the larger the maximum damping ratio, and the smaller the optimal damper coefficient. When $\gamma_M x_d/l$ is equal to 0.2, i.e., γ_M for $x_d/l=0.02$, the maximum damping ratio is increased by more than 20% of the original, from 0.51 to 0.64; and the normalized optimal damper coefficient is decreased by 20%, from 0.10 to 0.08. When $\gamma_M x_d/l$ is equal to 0.4, i.e., γ_M = 20 for $x_d/l=0.02$, the maximum damping ratio is increased by 60%, and the normalized optimal damper coefficient is decreased by 40%. In this case, ignoring the effect of damper mass will lead to overestimation of the

optimal damper coefficient. Recalling the definition of γ_M in Eq. (21) and noting that the abscissa shown in Fig. 8 is $\gamma_M x_d/l$, it is known that the effect of damper mass will become more significant for higher modes and when x_d/l is larger. Good agreement between the asymptotic results and the numerical ones validates Eqs. (64) to (66).

4.3 Stiffness of damper support

As aforementioned, softening of the damper support (increase of $\frac{1}{u_s}=0$) will decrease the maximum attainable damping ratio. However, two issues still remain to be addressed: (i) for a given cable-damper system, how large u_s should be to avoid an obvious reduction in control effectiveness, and (ii) how much the damping of the cable-damper system will be affected by a given support stiffness.

For brevity and without losing generality, the case of u_k = 0 and $\gamma_M=0$ is discussed here. In this case Eq. (42) can be written as

$$\frac{\xi_n}{\frac{x_d}{l}}=\frac{n\pi(\eta_c+\eta_I)S^2\frac{x_d}{l}}{1+\left[n\pi(\eta_c+\eta_I)\left(\frac{1}{u_sCS\frac{x_d}{l}}+1\right)CS\frac{x_d}{l}\right]^2} \tag{67}$$

When $\frac{1}{u_s}=0$, we have

$$\frac{\xi_n}{\frac{x_d}{l}}\left|\left(\frac{1}{u_s},u_k,\gamma_M=0\right)=\frac{n\pi(\eta_c+\eta_I)S^2\frac{x_d}{l}}{1+\left[n\pi(\eta_c+\eta_I)CS\frac{x_d}{l}\right]^2}\right. \tag{68}$$

By comparing Eqs. (67) and (68), the difference between the two equations is found to be only that *CS* is replaced by $\left(\frac{1}{u_sCS\frac{x_d}{l}}+1\right)CS$. The maximum damping ratio and the optimal damper coefficient in the case of u_k = 0 and $\gamma_M=0$ can be obtained from Eqs. (45) and (48) as

$$\frac{\xi_{n,opt}}{\frac{x_d}{l}}=\frac{S^2}{2CS}\frac{1}{\left(1+\frac{1}{u_sCS\frac{x_d}{l}}\right)}=\frac{\xi_{n,opt}}{\frac{x_d}{l}}\left|(u_s=0)\frac{1}{\left(1+\frac{1}{u_sCS\frac{x_d}{l}}\right)}\right. \tag{69}$$

$$\begin{aligned}(\eta_c+\eta_I)_{opt}&=\frac{1}{n\pi\left(\frac{1}{u_s\frac{x_d}{l}}+CS\right)\frac{x_d}{l}}\\&=(\eta_c+\eta_I)_{opt}\left|(u_s=0)\frac{1}{\left(1+\frac{1}{u_sCS\frac{x_d}{l}}\right)}\right.\end{aligned} \tag{70}$$

and the normalized optimal damper coefficient is

$$\kappa_{opt}=\frac{1}{\pi^2CS\left(1+\frac{1}{u_sCS\frac{x_d}{l}}\right)} \tag{71}$$

Softening of the support stiffness (increase of $\frac{1}{u_s}$) not only decreases the optimal damper coefficient, but also decreases the maximum attainable damping ratio.

Comparing Eqs. (67) and (68) and examining Eq. (69), in order not to obviously reduce the damping performance, u_s should satisfy

$$\frac{1}{u_s\frac{x_d}{l}}\le 0.1 \quad \text{or} \quad u_s\ge\frac{10}{\frac{x_d}{l}} \tag{72}$$

because $CS\approx 1$ in most situations. Recalling the definition of u_s in Eq. (21), the criterion given in Eq. (72) can be expressed as

$$\frac{T_0}{k_sx_d}\le 0.1 \quad \text{or} \quad k_s\ge\frac{10T_0}{x_d} \tag{73}$$

Fig. 9 shows the effect of support stiffness on the normalized damping ratio $\xi/(x_d/l)$ versus the normalized damper coefficient κ for the second mode when $\frac{x_d}{l}=0.02$, $\gamma_M=0$ and u_k = 0. Plotted in Fig. 9(a) are the results obtained by the numerical procedure for the support stiffness $\frac{1}{u_s}$ = 0, 0.001, 0.002, …, 0.012, respectively, with an arrow indicating the trend of increasing $\frac{1}{u_s}$. The line with dots links the peak points of the curves, indicating the change in the maximum damping ratio and the optimal damper coefficient. Softening of the support stiffness decreases not only the optimal damper coefficient, but also the maximum damping ratio. Fig. 9(b) gives a comparison of the asymptotic and numerical solutions for $\frac{1}{u_s}$ = 0, 0.004, 0.008, and 0.012. Good coincidence between them is observed.

Fig. 10 shows the effect of support stiffness on the maximum damping ratio and the optimal damper coefficient. It is observed that both the maximum damping ratio and the normalized optimal damper coefficient decrease parabolically with the increase of $1/(u_s x_d/l)$. The larger $1/(u_s x_d/l)$ is, the smaller the maximum damping ratio and the optimal damper coefficient. When $1/(u_s x_d/l)=0.1$, i.e. $\frac{1}{u_s}=0.0002$ for x_d/l = 0.02, the maximum damping ratio is decreased by 10% of the original, from 0.51 to 0.46; and the normalized optimal damper coefficient is also decreased by 10%, from 0.10 to 0.09. Therefore, to avoid an obvious deterioration of the system damping performance, the damper support should be designed to satisfy $1/(u_s x_d/l)\le 0.1$.

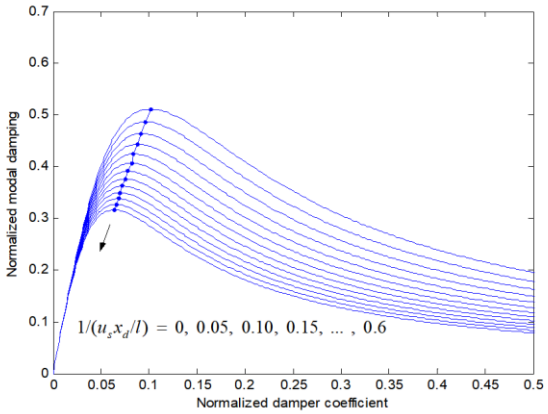

(a) Numerical solution

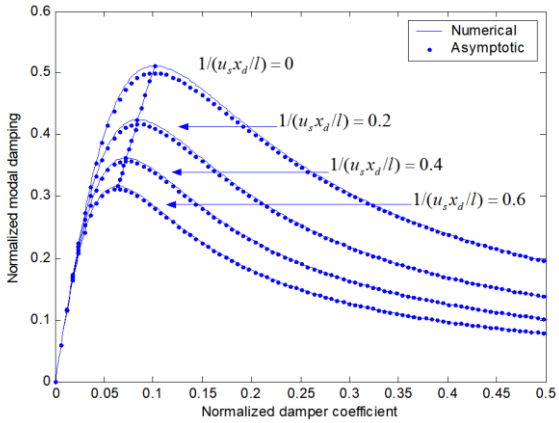

(b) Comparison of numerical and asymptotic solutions

Fig. 9 Effect of damper stiffness on 'universal curve' (x_d/l = 0.02, 2nd mode)

When $1/(u_s\, x_d\, /\, l)$ is up to 0.6, i.e., $\frac{1}{u_s} = 0.0012$ for x_d/l = 0.02, both the maximum damping ratio and the normalized optimal damper coefficient are decreased by 40%. In this case, ignoring the effect of support stiffness will lead to severe overestimation of both the maximum attainable damping ratio and the optimal damper coefficient. Good agreement between the asymptotic and numerical solutions validates Eqs. (69) to (71).

4.4 Combined effect

The effects of damper stiffness, damper mass, and support stiffness should be jointly investigated when u_k ,γ_M , and u_s are not zero. Eq. (37) can be expressed as

$$\frac{\xi_n}{\frac{x_d}{l}} = \frac{n\pi(\eta_c+\eta_I)S^2\frac{x_d}{l}}{\left[1+U_{k,M,s}+U_{k,M}\right]^2+\left[n\pi(\eta_c+\eta_I)V_{M,s}CS\frac{x_d}{l}\right]^2} \tag{74}$$

where

$$U_{k,M,s} = \frac{u_k}{u_s}(1-\gamma_M CS\frac{x_d}{l}) \tag{75}$$

$$U_{k,M} = (u_k-\gamma_M)CS\frac{x_d}{l} \tag{76}$$

$$V_{M,s} = \left(\frac{1}{u_s}(1-\gamma_M CS\frac{x_d}{l})+CS\frac{x_d}{l}\right)\Big/\left(CS\frac{x_d}{l}\right) \tag{77}$$

In the above, $U_{k,M,s}$ is a factor accounting for the coupled effect of the damper stiffness u_k , damper mass γ_M , and support stiffness u_s ; $U_{k,M}$ is a factor accounting for the coupled effect of u_k and γ_M ; and $V_{M,s}$ is a factor accounting for the coupled effect of γ_M and u_s . Eq. (74) is a general formula for designing MR dampers to achieve optimal open-loop vibration control of taut cables.

The maximum attainable damping ratio and the optimal damper coefficient can be easily obtained from Eq. (74) as

$$\xi_{n,opt} = \xi_{n,opt}\Big|_{(\frac{1}{u_s},u_k,\gamma_M=0)}\frac{1}{V_{M,s}(1+U_{k,M,s}+U_{k,M})} \tag{78}$$

$$(\eta_c+\eta_I)_{opt} = (\eta_c+\eta_I)_{opt}\Big|_{(\frac{1}{u_s},u_k,\gamma_M=0)}\cdot\frac{1+U_{k,M,s}+U_{k,M}}{V_{M,s}} \tag{79}$$

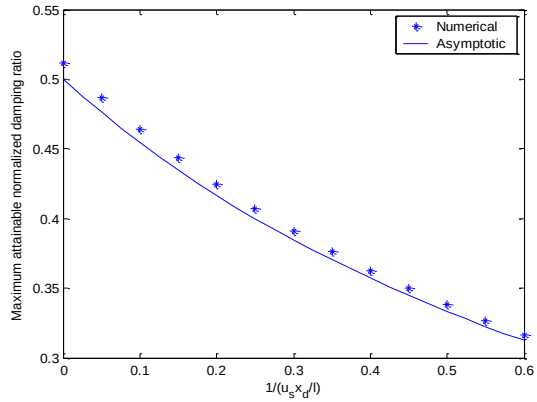

(a) Maximum attainable damping ratio

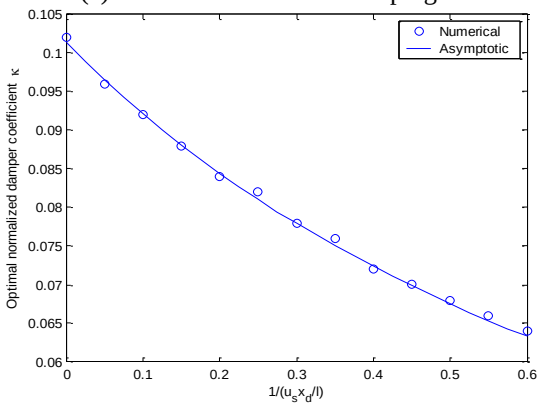

(b) Optimal damper coefficient

Fig. 10 Effect of damper stiffness on damping performance (x_d/l = 0.02, 2nd mode)

From Eqs. (78) and (79), the affecting factors $U_{k,M,s}$ and $U_{k,M}$ tend to decrease the maximum damping ratio by multiplying $\frac{1}{(1+U_{k,M,s}+U_{k,M})}$ and to increase the optimal damper coefficient by multiplying $(1+U_{k,M,s}+U_{k,M})$, while the affecting factor $V_{M,s}$ tends to decrease both the maximum damping ratio and the optimal damper coefficient by multiplying $\frac{1}{V_{M,s}}$. By defining the following correction coefficients

$$\Gamma_{\xi}=\frac{1}{V_{M,s}(1+U_{k,M,s}+U_{k,M})} \tag{80}$$

$$\Gamma_{\eta}=\frac{1+U_{k,M,s}+U_{k,M}}{V_{M,s}} \tag{81}$$

Eqs. (78) and (79) can be simplified as

$$\xi_{n,opt}=\xi_{n,opt}\Big|_{(\frac{1}{u_s},u_k,\gamma_M=0)}\Gamma_{\xi} \tag{82}$$

$$(\eta_c+\eta_I)_{opt}=(\eta_c+\eta_I)_{opt}\Big|_{(\frac{1}{u_s},u_k,\gamma_M=0)}\Gamma_{\eta} \tag{83}$$

Recalling the definition of the normalized damper coefficient in Eq. (56), we have

$$\kappa_{opt}=\kappa_{opt}\Big|_{(\frac{1}{u_s},u_k,\gamma_M=0)}\Gamma_{\eta} \tag{84}$$

The expressions of $\xi_{n,opt}$, $(\eta_c+\eta_I)_{opt}$, and κ_{opt} when $\frac{1}{u_s}$, u_k, and γ_M are all zero are given as

$$\frac{\xi_{n,opt}\Big|_{(\frac{1}{u_s},u_k,\gamma_M=0)}}{\frac{x_d}{l}}=\frac{S^2}{2CS} \tag{85}$$

$$(\eta_c+\eta_I)_{opt}\Big|_{(\frac{1}{u_s},u_k,\gamma_M=0)}=\frac{1}{n\pi CS\frac{x_d}{l}} \tag{86}$$

$$\kappa_{opt}\Big|_{(\frac{1}{u_s},u_k,\gamma_M=0)}=\frac{1}{\pi^2 CS} \tag{87}$$

After so doing, the combined effect of damper stiffness, damper mass, and support stiffness can be readily investigated by observing the two correction coefficients Γ_{ξ} and Γ_{η}. The variation of Γ_{ξ} and Γ_{η} with the normalized damper stiffness ($u_k\frac{x_d}{l}$), the normalized damper mass ($\gamma_M\frac{x_d}{l}$), and the normalized support stiffness $1/(u_s\frac{x_d}{l})$ is shown in Fig. 11. It is seen that Γ_{ξ} increases with ($\gamma_M\frac{x_d}{l}$) but decreases with ($u_k\frac{x_d}{l}$) and $1/(u_s\frac{x_d}{l})$. When $u_k\frac{x_d}{l}=0$, $1/(u_s\frac{x_d}{l})=0$, and $(\gamma_M\frac{x_d}{l})=0.4$, Γ_{ξ} equals 1.67 which corresponds to the maximum normalized damping ratio $\frac{\xi_{opt}}{\frac{x_d}{l}}=\frac{1}{2}\times\Gamma_{\xi}=0.84$. Hence, to make the maximum attainable damping ratio higher, we should eliminate the damper stiffness, make the support stiff enough, and utilize the benefit of the damper mass. The correction coefficient Γ_{η} increases with ($u_k\frac{x_d}{l}$), but decreases with $1/(u_s\frac{x_d}{l})$ and ($\gamma_M\frac{x_d}{l}$). As an example, when $1/(u_s\frac{x_d}{l})=0$, $(\gamma_M\frac{x_d}{l})=0$, and $(u_k\frac{x_d}{l})=1.0$, Γ_{η} equals 2.0 which corresponds to the optimal normalized damper coefficient $\kappa_{opt}=0.2$ (twice of that without damper stiffness).

5. Conclusions

In this paper, an analysis method for open-loop vibration control of taut cables using MR dampers has been developed.

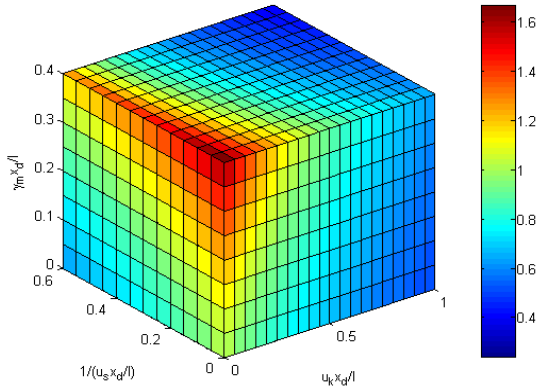

(a) Γ_{ξ}

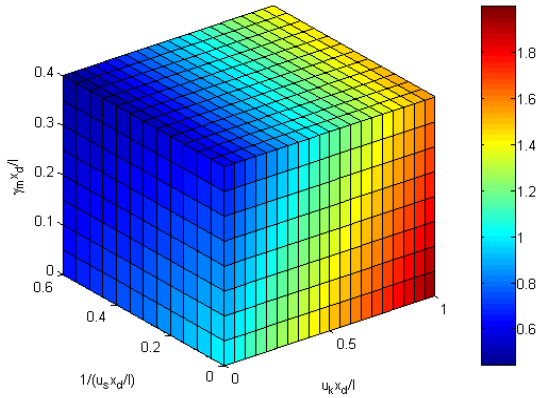

(b) Γ_{η}

Fig. 11 Correction coefficients versus damper stiffness, damper mass, and support stiffness

Both numerical and asymptotic solutions are obtained to evaluate the system maximum damping ratio and the optimal damper coefficient. The individual effects of damper stiffness, damper mass and stiffness of damper support on the cable damping performance are first investigated in detail. Then the combined effect of damper stiffness, damper mass and stiffness of the damper support is analyzed by defining two correction coefficients that can quantitatively predict the influence of the above parameters on the maximum damping ratio and the optimal damper coefficient. The derived general formula facilitates the design of MR dampers to achieve optimal open-loop vibration control of taut cables.

It turns out that the damper stiffness decreases the maximum attainable damping ratio and increases the optimal damper coefficient; the damper mass counteracts the effect of the damper stiffness and may increase the maximum attainable damping ratio when the damper mass is appropriate; and softening of the support stiffness decreases both the maximum attainable damping ratio and the optimal damper coefficient. As a result, one should endeavor to eliminate damper stiffness, make damper support stiff enough, and utilize the benefit of damper mass in designing MR dampers for cable vibration control. To attain the maximum damping ratio for all cables on a cable-stayed bridge, voltage/current input to the MR dampers should be adjusted with the optimal damper coefficient specific for each cable.

Even through, this study is initiated for MR dampers, but it is applicable for general external dampers for cable vibration mitigation, such as the electro-rheological dampers (Powell 1994), and inertial mass dampers (Lu *et al.* 2017, Wang *et al.* 2019), and so on. Extension of this study to sagged cables is presented in the paper (Duan *et al.* 2019).

Acknowledgments

This research work was supported by the National Natural Science Foundation of China (U1709216, 51578419, 51522811, 51478429, and 90915008)，the National Key R&D Program of China (2017YFC0806100), the grant from the Ministry of Science and Technology of China (Grant No. 2018YFE0190100) the grant from the Research Grants Council of the Hong Kong Special Administrative Region, China (Project No. PolyU 5252/07E), and the grant from The Hong Kong Polytechnic University through the Development of Niche Areas Programme (Project No. 1-BB95).

References

Butz, T. and von Stryk, O. (2002), "Modelling and simulation of electro- and magnetorheological fluid dampers", *ZAMM-Zeitschrift für Angewandte Mathematik und Mechanik*, **82**(1), 3-20. https://doi.org/10.1002/1521-4001(200201)82:1<3::AID-ZAMM3>3.0.CO;2-O.

Chen, Z.H., Lam, K.H. and Ni, Y.Q. (2016), "Enhanced damping for bridge cables using a self-sensing MR damper", *Smart Mater. Struct.*, **25**(8), 085019.

Chen, Z.Q., Wang, X.Y., Ko, J.M., Ni, Y.Q., Spencer, B.F., Jr., Yang, G. and Hu, J.H. (2004), "MR damping system for mitigating wind-rain induced vibration on Dongting Lake Cable-Stayed Bridge", *Wind Struct.*, **7**(5), 293-304. http://dx.doi.org/10.12989/was.2004.7.5.293.

Duan, Y.F. (2004), *Vibration Control of Stay Cables Using Semi-active Magneto-rheological (MR) Dampers*, PhD thesis, Hong Kong: Department of Civil and Structural Engineering, The Hong Kong Polytechnic University, Hong Kong.

Duan, Y.F., Ni, Y.Q. and Ko, J.M. (2006), "Cable vibration control using Magneto-rheological (MR) dampers", *J. Intel. Mat. Syst. Str.*, **17**(4), 321-325. https://doi.org/10.1142/9789812702197_0121.

Duan, Y.F., Ni, Y.Q. and Ko, J.M. (2005), "State-derivative feedback control of cable vibration using semiactive magnetorheological dampers", *Comput.-Aided Civil Infrastruct. Eng.*, **20**, 431-449. https://doi.org/10.1111/j.1467-8667.2005.00396.x.

Duan, Y.F., Ni, Y.Q., Zhang, H.M., Spencer, B.F., Jr., Ko, J.M. and Dong S.H. (2019), "Design formulas for vibration control of sagged cables using passive MR dampers", *Smart Struct. Syst.*, Accepted.

Duan, Y.F., Tao, J.J., Zhang, H.M., Wang, S.M. and Yun C.B. (2018), "Real-time hybrid simulation based on vector form intrinsic finite element and field programmable gate array", *Struct. Control Health Monit.*, **26**(1), e2277; https://doi.org/10.1002/stc.2277.

Guan, X.C., Huang Y., Li, H. and Ou, J.P. (2012), "Adaptive MR damper cable control system based on piezoelectric power harvesting", *Smart Struct. Syst.*, **10**(1), 33-46. https://doi.org/10.12989/sss.2012.10.1.033.

Hikami, Y. and Shiraishi, N. (1988), "Rain−wind induced vibrations of cables in cable stayed bridges", *J. Wind Eng. Ind. Aerod.*, **29**, 409-418.

Huang, H.W., Liu, J.Y. and Sun, L.M. (2015), "Full-scale experimental verification on the vibration control of stay cable using optimally tuned MR damper", *Smart Struct. Syst.*, **16**(6), 1003-1021. https://doi.org/10.12989/sss.2015.16.6.1003.

Huang, H.W., Sun, L.M and Jiang X.L. (2012), "Vibration mitigation of stay cable using optimally tuned MR damper", *Smart Struct. Syst.*, **9**(1), 35-53. http://dx.doi.org/10.12989/sss.2012.9.1.035.

Huang, Z.H. and Jones N.P. (2011), "Damping of taut-cable systems: effects of linear elastic spring support", *J. Eng. Mech.*, **137**(7), 512-518. https://doi.org/10.1061/(ASCE)EM.1943-7889.0000252.

Irwin, P.A. (1997), "Wind vibrations of cables on cable-stayed bridges", (Eds., Kempner, L. Jr., and Brown, C.B.), editors. *Building to Last Structures Congress: Proceedings of the 15th Structures Congress, New York: American Society of Civil Engineers*, 383-387.

Johnson, E.A., Baker, G.A., Spencer Jr. B.F. and Fujino, Y. (2007), "Semiactive damping of stay cables", *J. Eng. Mech. - ASCE*, **133**, 1-11. https://doi.org/10.1061/(ASCE)0733-9399(2007)133:1(1).

Johnson, E.A., Christenson, R.E. and Spencer, Jr. B.F. (2003), "Semiactive damping of cables with sag", *Comput. - Aided Civil Infrastruct. Eng.*, **18**(2), 132-146. https://doi.org/10.1111/1467-8667.00305.

Johnson, E.A., Spencer, Jr. B.F. and Fujino, Y. (1999), "Semiactive damping of stay cables: a preliminary study", *Proceedings of the 17th International Modal Analysis Conference, Society for Experimental Mechanics*, 417-423.

Jung, H.J., Spencer, Jr. B.F., Ni, Y.Q. and Lee, I.W. (2004), "State-of-the-art of semiactive control systems using MR fluid dampers in civil engineering applications", *Struct. Eng. Mech.*,

17, 493-526. http://dx.doi.org/10.12989/sem.2004.17.3_4.493.

Kim, I.H., Jung, H.J. and Koo J.H. (2010), "Experimental evaluation of a self-powered smart damping system in reducing vibrations of a full-scale stay cable", *Smart Mater. Struct.*, **19**(11), 11527.

Ko, J.M., Ni, Y.Q., Chen, Z.Q. and Spencer, Jr. B.F. (2003), "Implementation of MR dampers to Dongting Lake Bridge for cable vibration mitigation", *In: Casciati F, editor. Proceedings of the 3rd World Conference on Structural Control, Chichester, England: John Wiley & Sons*, 777-786.

Kovacs, I. (1982), "Zur Frage der seilschwingungen und der seildampfung", *Die Bautechnik*, **10**, 325-332, (in German).

Krenk, S. (2004), "Complex modes and frequencies in damped structural vibrations", *J. Sound Vib.*, **270**(4-5), 981-996. https://doi.org/10.1016/S0022-460X(03)00768-5.

Krenk, S. (2000), "Vibrations of a taut cable with an external damper", *J. Appl. Mech. – ASME*, **67**(4), 772-776. doi:10.1115/1.1322037.

Krenk, S. and Høgsberg, J.R. (2005), "Damping of cables by a transverse force", *J. Eng. Mech. – ASCE*, **131**, 340-348. https://doi.org/10.1061/(ASCE)0733-9399(2005)131:4(340).

Krenk, S. and Nielsen, S.R.K. (2002), "Vibrations of a shallow cable with a viscous damper", *Proceedings of the Royal Society of London, Series A*, **458**, 339-357. https://doi.org/10.1098/rspa.2001.0879

Li, H., Liu, M., Li, J.H., Guan, X.C. and Ou, J.P. (2007), "Vibration control of stay cables of the Shandong Binzhou Yellow River Highway Bridge using Magnetorheological fluid dampers", *J. Bridge Eng.*, **12**(4), 401-409. https://doi.org/10.1061/(ASCE)1084-0702(2007)12:4(401).

Lu, L. and Duan, Y.F., Spencer, B.F. Jr., Lu, X.L. and Zhou, Y. (2017), "Inertial mass damper for mitigating cable vibration", *Structural Control Health Monit.*, **24**, e1986, doi: 10.1002/stc.1986.

Main, J.A. and Jones, N.P. (2001), "Evaluation of viscous dampers for stay-cable vibration mitigation", *J. Bridge Eng. - ASCE*, **6**(6), 385-397. https://doi.org/10.1061/(ASCE)1084-0702(2001)6:6(385).

Main, J.A. and Jones, N.P. (2002a), "Free vibrations of taut cable with attached damper. I: linear viscous damper", *J. Eng. Mech. - ASCE*, **128**(10), 1062-1071. https://doi.org/10.1061/(ASCE)0733-9399(2002)128:10(1062).

Main, J.A. and Jones, N.P. (2002b), "Free vibrations of taut cable with attached damper. II: Nonlinear damper", *J. Eng. Mech. - ASCE*, **128**(10), 1072-1081. https://doi.org/10.1061/(ASCE)0733-9399(2002)128:10(1072).

Matsumoto, M., Saitoh, T., Kitazawa, M., Shirato, H. and Nishizaki, T. (1995), "Response characteristics of rain-wind induced vibration of stay-cables of cable- stayed bridges", *J. Wind Eng. Ind. Aerod.*, **57**(2-3), 323-333. https://doi.org/10.1016/0167-6105(95)00010-O.

Matsumoto, M., Shiraishi, N. and Shirato, H. (1992), "Rain-wind induced vibration of cables of cable-stayed bridges", *J. Wind Eng. Ind. Aerod.*, **41-44**, 2011−22. https://doi.org/10.1016/0167-6105(92)90628-N.

Miyata, T. (1991), "Design considerations for wind effects on long-span cable-stayed bridges", *(Eds., Ito, M., Fujino, Y., Miyata, T., Narita, N.), Cable-Stayed Bridges: Recent Developments and their Future, Amsterdam: Elsevier*, 235-256.

Ni, Y.Q., Chen, Y., Ko, J.M. and Cao, D.Q. (2002), "Neuro-control of cable vibration using semi-active magneto-rheological dampers", *Eng. Struct.*, **24**(3), 295-307. https://doi.org/10.1016/S0141-0296(01)00096-7.

Ni, Y.Q., Wang, X.Y., Chen, Z.Q. and Ko, J.M. (2007), "Field observations of rain-wind-induced cable vibration in cable-stayed Dongting Lake Bridge", *J. Wind Eng. Ind. Aerod.*, **95**(5), 303-328. https://doi.org/10.1016/j.jweia.2006.07.001.

Or, S.W., Duan, Y.F., Ni, Y.Q., Chen, Z.H. and Lam, K.H. (2008), "Development of Magnetorheological dampers with embedded piezoelectric force sensors for structural vibration control", *J. Intel. Mat. Syst. Str.*, **19** (11), 1327-1338. https://doi.org/10.1177/1045389X07085673.

Ou, J.P. (2003), "Some recent advances of intelligent health monitoring systems for civil infrastructures in mainland China", *(Eds., Wu, Z.S. and Abe, M.), Structural Health Monitoring and Intelligent Infrastructure, Netherlands: Balkema*, 131-144.

Pacheco, B.M. and Fujino, Y. (1993), "Keeping cables calm", *ASCE Civil Eng.*, **63**(10), 56-58.

Pacheco, B.M., Fujino, Y. and Sulekh, A. (1993), "Estimation curve for modal damping in stay cables with viscous damper", *J. Struct. Eng.- ASCE*, **119**, 1961-1979.

Persoon, A.J. and Noorlander, K. (1999), "Full-scale measurements on the Erasmus Bridge after rain/wind induced cable vibrations", *(Eds., Larsen, A., Larose, G.L. and Livesey, F.M.), Wind Engineering into the 21st Century. Rotterdam: Balkema*, 1019-1926.

Poston, R.W. (1998), "Cable-stay conundrum", *ASCE Civil Eng.*, **68**(8), 58-61.

Powell, J.A. (1994), "Modeling the oscillatory response of an electrorheological fluid", *Smart Mater. Struct.*, **3**(4), 416-438.

Spencer, Jr. B.F., Dyke, S.J., Sain, M.K. and Carlson, J.D. (1997), "Phenomenological model for magnetorheological dampers", *J. Eng. Mech. - ASCE*, **123**(3), 230-238. https://doi.org/10.1061/(ASCE)0733-9399(1997)123:3(230).

Sulekh, A. (1990), *Non-Dimensionalized Curves for Modal Damping in Stay Cables with Viscous Dampers*, Master thesis, Japan: Department of Civil Engineering, University of Tokyo.

Tanaka, H. (2003), "Aerodynamics of cables", *Proceedings of the 5th International Symposium on Cable Dynamics*. *Belgium: AIM*, 11-25.

Takano, H., Ogasawara, M., Ito, N., Shimosato, T., Takeda, K. and Murakami, T. (1997), "Vibrational damper for cables of the Tsurumi Tsubasa Bridge", *J. Wind Eng. Ind. Aerod.*, **69-71**, 807-818. https://doi.org/10.1016/S0167-6105(97)00207-9.

Verwiebe, C. (1998), "Rain−wind-induced vibrations of cables and bars", *(Eds., Larsen, A. and Esdahl, S.), Bridge Aerodynamics: Proceedings of the International Symposium on Advances in Bridge Aerodynamics. Rotterdam: Balkema*, 255-263.

Virlogeux, M. (1998), "Cable vibrations in cable-stayed bridges", *(Eds., Larsen, A. and Esdahl, S.), Bridge aerodynamics: Proceedings of the International Symposium on Advances in Bridge Aerodynamics. Rotterdam: Balkema*, 213-233.

Wang, Z.H., Chen, Z.H., Gao, H. and Wang, H. (2018), "Development of a self-powered magnetorheological damper system for cable vibration control", *Appl. Sci. -Basel*, **8**(1), 118. https://doi.org/10.3390/app8010118.

Wang, Z.H, Xu, Y.W., Gao, H., Chen, Z.Q., Xu, K. and Zhao S.B. (2019), "Vibration control of a stay cable with a rotary electromagnetic inertial mass damper", *Smart Struct. Syst.*, Accepted.

Wang, W., Hua, X. and Wang X. (2019), "Mechanical behavior of magnetorheological dampers after long-term operation in a cable vibration control system", *Struct. Control Health Monit.*, **26**(1), e2280. https://doi.org/10.1002/stc.2280.

Wang, X.Y., Ni, Y.Q., Ko, J.M. and Chen, Z.Q. (2005), "Optimal design of viscous dampers for multi-mode vibration control of bridge cables", *Eng. Struct.*, **27**(5), 792-800. https://doi.org/10.1016/j.engstruct.2004.12.013.

Watson, S.C. and Stafford, D. (1988), "Cables in trouble", *ASCE Civil Eng.*, **58**(4), 138-141.

Weber, F., Bhowmik, S. and Hogsberg, J. (2014), "Extended neural network-based scheme for real-time force tracking with magnetorheological dampers", *Struct. Control Health Monit.*, **21**(2), 225-247. https://doi.org/10.1002/stc.1569.

Weber, F. and Boston, C. (2010), "Energy based optimization of viscous-friction dampers on cables", *Smart Mater. Struct.*, **19**(4), 045025.

Weber, F., Distl, H. and Feltrin, G. (2009), "Cycle energy control of magnetorheological dampers on cables", *Smart Mater. Struct.*, **18**(1), 015005.

Wu, W.J. and Cai, C.S. (2010), "Cable vibration control with a semiactive MR damper-numerical simulation and experimental verification", *Struct. Eng. Mech.*, **34**(5), 611-623. https://doi.org/10.12989/sem.2010.34.5.611.

Xu, Y.L. and Zhou, H.J. (2007), "Damping cable vibration for a cable-stayed bridge using adjustable fluid dampers", *J. Sound Vib.*, **306**(1-2), 349-360. https://doi.org/10.1016/j.jsv.2007.05.032

Yamada, H. (1997), "Control of wind-induced cable vibrations from a viewpoint of the wind resistant design of cable-stayed bridges", *Proceedings of International Seminar on Cable Dynamics. Tokyo: Japan Association for Wind Engineering*, 129-138.

Yamaguchi, H. and Fujino, Y. (1998), "Stayed cable dynamics and its vibration control. In: Larsen A., Esdahl S, editors", *Bridge aerodynamics: Proceedings of the International Symposium on Advances in Bridge Aerodynamics. Rotterdam: Balkema*, 235-253.

Zhao, M. and Zhu, W.Q. (2011), "Stochastic optimal semi-active control of stay cables by using magneto-rheological damper", *J. Vib. Control*, **17**(13), 1921-1929. https://doi.org/10.1177/1077546310371263.

Zhou, H.J., Huang X.J., Xiang N., He J.W., Sun, L.M. and Xing, F. (2018), "Free vibration of a taut cable with a damper and a concentrated mass", *Struct. Control Health Monit.*, **25**(11), 1-21. https://doi.org/10.1002/stc.2251.

Zhou, H.J., Xiang, N. and Huang, X. (2018), "Full-scale test of dampers for stay cable vibration mitigation and improvement measures", *Struct. Monit. Maint.*, **5**(4), 489-506. https://doi.org/10.12989/smm.2018.5.4.489.

Zhou, H.J. and Sun, L.M. (2013), "Damping of stay cable with passive-on magnetorheological dampers: a full-scale test", *Int. J. Civil Eng.*, **11**(3), 154-159.

Zhou, H.J., Sun, L.M. and Xing, F. (2014), "Damping of full-scale stay cable with viscous damper: experiment and analysis", *Adv. Struct. Eng.*, **17**(2), 265-274. https://doi.org/10.1260/1369-4332.17.2.265.